ACS Catalysis

Research Article

pubs.acs.org/acscatalysis

Nanoscale Transformations of Alumina-Supported AuCu Ordered Phase Nanocrystals and Their Activity in CO Oxidation

Sharif Najafishirtari, Rosaria Brescia, Pablo Guardia,† Sergio Marras, Liberato Manna,* and Massimo Colombo*

Department of Nanochemistry, Istituto Italiano di Tecnologia, Via Morego 30, 16163 Genova, Italy

Supporting Information

ABSTRACT: In this work we applied colloidal preparation methods to synthesize AuCu nanocrystals (NCs) in the ordered tetragonal phase with an atomic composition close to 50:50. We deposited the NCs on a support (Al_2O_3), studied their transformations upon different redox treatments, and evaluated their catalytic activity in the CO oxidation reaction. The combined analyses by energy dispersive X-ray spectroscopy (EDX)-scanning transmission electron microscopy (STEM), selected area electron diffraction (SAED), and in situ diffuse reflectance infrared Fourier transform spectroscopy (DRIFTS) highlighted a phase segregation between gold and copper upon the high-temperature (350 °C) oxidizing treatment. While gold remained localized in the NCs, copper was finely dispersed on the support, likely in the form of oxide clusters. AuCu alloyed NCs, this time in the form of solid solution, face-centered cubic phase, were then restored upon a reducing treatment at the same temperature, and their catalytic activity was significantly enhanced in comparison to that of the oxidized system. The composition of the NCs and consequently the CO oxidation reaction rate were also affected by the CO/O_2 reacting atmosphere: regardless of the pretreatment, the same catalytic activity was approached over time on stream at temperatures as low as 100 °C. Consistently, the same situation was observed on the catalyst surface as probed by EDX-STEM, SAED, and DRIFTS. All of these transformations were found to be fully reversible.

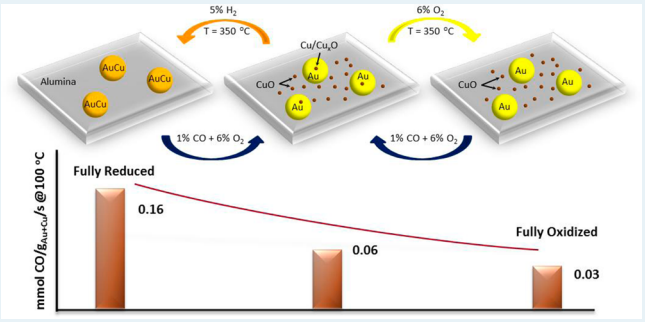

KEYWORDS: *AuCu, bimetallic nanocrystals, nanoalloy, CO oxidation, DRIFTS*

1. INTRODUCTION

Bimetallic nanocrystals (NCs) have caught researchers' attention in catalysis over the past decade.[1] While conventional preparation methods have been extensively applied to provide bimetallic catalysts with enhanced performances, the use of NCs in catalyst preparation offers the additional possibility to finely tune the size and the composition of the metallic active sites and to exploit synergetic effects between different metals.[1a] Such a synergy is usually the result of electronic or structural modifications of the active sites arising from interactions among metals (such as alloying) at the nanoscale, which can eventually result in a material with enhanced catalytic properties.[1c] Bimetallic catalysts composed of Au and a secondary metal are among the most widely studied materials in heterogeneous catalysis, with particular interest in CO oxidation.[2] The presence of a base metal such as Ag, Ni, Co, or Cu[2a,3] can indeed facilitate electron transfer to oxygen molecules while maintaining good CO adsorption capacity in comparison to monometallic Au and thus enhancing the catalytic activity.[3f] As an example, catalysts based on Au−Cu alloys have been reported to be promising and effective in low-temperature CO oxidation, as they exhibit higher activity and resistance against sintering in comparison to monometallic Au catalysts.[3a,b,d,4] On the other hand, the effect of redox treatments on bimetallic AuCu catalysts and the resulting changes in the catalytic activity toward CO oxidation are still debated in the scientific literature, and conflicting results have been reported.

Liu et al.[4b] prepared a Au-Cu/SBA-15 catalyst by means of consecutive reduction of Au and Cu precursors and studied the structural changes of the prepared catalyst in different conditions. They reported that, when Cu was in the form of an oxide and was attached to the Au NCs as a layer or patches of CuO, the catalyst was highly active in the CO oxidation. In contrast, the catalyst was inactive when Cu in the metallic state was alloyed with Au. The effectiveness of Cu oxide species in the bimetallic Au-Cu catalyst used in oxidation reactions has been reported in other works as well.[3d,e,4a,b,5] Mozer et al.[3c] studied the effect of Cu loading on the CO oxidation activity of an alumina-supported Au catalyst prepared by deposition−precipitation. The authors showed that there was a correlation between activity and Cu loading. While low amounts of copper were beneficial for the CO oxidation activity, high copper contents caused blocking of the Au active sites, thus decreasing the catalytic activity. Sandoval et al.[3d] prepared a Au-Cu/TiO_2

Received: December 2, 2014
Revised: February 6, 2015
Published: February 23, 2015

DOI: 10.1021/cs501923x
ACS Catal. 2015, 5, 2154−2163

catalyst by sequential deposition−precipitation and studied the effect of the Au/Cu ratio and of the activation treatment. They reported the highest activity in CO oxidation for the catalyst with a Au:Cu ratio of 1:0.9 after activation in air at 300 °C and attributed the high activity to the formation of an Au/CuO/TiO_2 structure. Bauer and co-workers[5] studied the effect of different pretreatments on the CO oxidation activity of AuCu catalysts formed by reduction and diffusion of Cu into Au NCs already supported on silica. They observed that the activity of ordered AuCu alloy NCs, formed by reducing the catalyst under an H_2 atmosphere, was negligible at room temperature but started increasing when the temperature reached the level at which the segregation of Cu and the formation of amorphous Cu oxide occurred. Consistently, a much higher CO oxidation activity was observed when the sample was pretreated in O_2 at high temperatures.

A different scenario was described by Yin et al.,[6] who thoroughly investigated the properties of AuCu alloyed NCs synthesized by both wet chemical methods and nanoscale alloying. They reported the activity of such NCs supported on carbon and silica in the CO oxidation. The catalyst with a $Au_{51}Cu_{49}$ composition, supported on C, was more active when exposed to a reducing treatment than to an oxidizing one, although for copper-rich NCs ($Au_{11}Cu_{89}$/C), the difference was not as significant. They claimed that the formation of a large number of surface oxygenated Cu species after the oxidizing pretreatment blocked the surface of Au NCs, thus inhibiting the CO oxidation. They did not observe phase segregation between Au and Cu.

Most of the reports mentioned above referred to AuCu catalysts that were obtained according to conventional preparation methods: for example, coprecipitation or coimpregnation. Although these methods are relatively simple and scalable, their main drawback is that they are often characterized by a poor control over NCs size and composition. Considering the complex transformations that nanoalloys undergo upon activation treatments and catalysis, a strong heterogeneity of the synthesized material can yield drastically different results. In order to overcome this limitation, in this work we followed colloidal preparation methods to synthesize size-tunable AuCu NCs of well-defined composition (Scheme 1 left, center left, and center right sketches). Colloidal synthesis indeed allowed the fine tuning of the NC size, shape, and composition at a level which is typically not achievable with classical catalyst preparation methods.[7] By means of colloidal deposition we effectively prepared an alumina-supported catalyst and studied the effect of different activation treatments on catalyst morphology, composition, and CO oxidation catalytic activity (Scheme 1, right image).

Scheme 1. Sketch of Seeded Growth Protocol for AuCu Colloidal NC Synthesis, Preparation of the Catalyst, and CO Oxidation Catalytic Tests: (Left) Reduction of the Starting Au^{3+} Precursor in Solution To Form (Center Left) Au NCs and Addition of a Cu^{2+} Precursor Leading to (Center Right) the Formation of AuCu NCs, Which Are Then Mixed with Alumina Grains To Prepare (Right) the Final Catalyst for the CO Oxidation Reaction

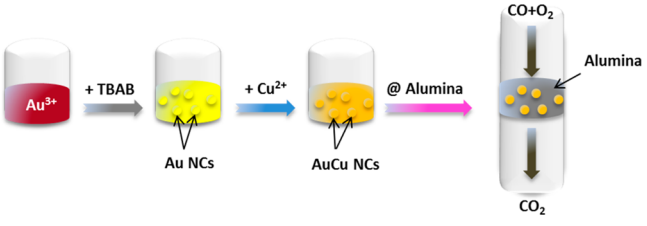

The exposure at high temperature (350 °C) to an oxidizing environment caused a phase segregation between gold and copper, which was found to be detrimental for the CO oxidation reaction. On the other hand, AuCu alloyed NCs were restored when the catalyst was exposed to a reducing environment and the catalytic activity was then significantly enhanced. The CO/O_2 reacting atmosphere also caused changes in the NC composition and consequently in the reaction rate: for a reduced system the catalytic activity progressively decreased with time on stream, as a consequence of Cu dealloying and of partial migration on the support surface. On the other hand, when starting from a fully oxidized situation, the reaction environment caused a partial realloying of Cu, which in turn resulted in the progressive increase of the catalyst activity. All of these transformations were found to be fully reversible.

2. RESULTS

2.1. Characterization of the as-Synthesized AuCu NCs.

Colloidal Au NCs were prepared by fast reduction of Au^{3+} at room temperature[8] and were kept suspended in hexane (see the Experimental Section). The uniformity of the as-synthesized NCs was verified by transmission electron microscopy (TEM, see Figure S1 in the Supporting Information). The size distribution was obtained by statistical size measurement including 450 particles (see the inset of Figure S1), which yielded an average particle size of 3.1 ± 0.4 nm, confirming a monodispersed size distribution, considering the criterion of having $\sigma \leq 15\%$.[9] These NCs were further used to prepare the AuCu NCs (atomic Au:Cu = 50:50) through a seed-based diffusion mechanism:[10] according to Chen et al.,[10] Cu^{2+} ions were reduced to highly active Cu^0 atoms or clusters by a mild reducing agent, i.e. oleylamine (OlAm), and reacted with the surface of Au NCs. The Cu atoms diffused then from the surface of the Au NCs to their interior, resulting in the formation of a AuCu solid solution. OlAm acted also as a stabilizing agent.[11] The size distribution of the as-synthesized AuCu NCs was estimated in a manner similar to that for the Au seeds, by measuring the sizes of 450 particles (Figure 1). Having a mean size of 6.1 ± 1.0 nm, it was concluded that the size distribution was narrow, according to the criterion of $\sigma \leq 20\%$.[9] Elemental mapping by means of scanning TEM-energy-dispersive X-ray spectroscopy (STEM-EDX) over several NCs indicated a homogeneous distribution of Au and Cu within each NC (see Figure 1e−h).

The composition of the alloy NCs was quantitatively analyzed by inductively coupled plasma atomic emission spectroscopy (ICP-AES) and scanning electron microscopy (SEM)-EDX: the first technique gave an atomic Au:Cu ratio of 53:47, while the second technique gave a ratio of 48:52 (see Figure S2 in the Supporting Information). Both values were close to the desired target of Au:Cu = 50:50. The ratio between the amount of copper in the final product and the amount of copper in the precursors was around 95%, thus highlighting the high yield of the applied synthesis protocol. X-ray diffraction patterns collected from the NCs (Figure 1d) were in agreement with a body-centered-tetragonal structure, corresponding to an ordered AuCu alloy, which was previously reported for Au:Cu atomic ratios of around 1.[10,12] SAED patterns collected from

DOI: 10.1021/cs501923x
ACS Catal. 2015, 5, 2154−2163

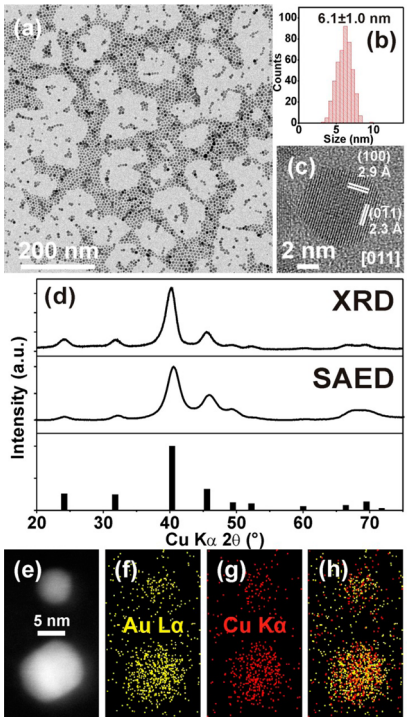

Figure 1. (a) Typical bright-field (BF)-TEM image of the as-prepared AuCu colloidal NCs. (b) Size distribution histogram obtained by measuring 450 NCs. (c) High-resolution TEM (HRTEM) image of a single AuCu NC matching with the [011] zone axis of tetragonal AuCu (JCPDS No. 01-071-5024). (d) X-ray diffraction (XRD) and azimuthally integrated, background-subtracted, selected area electron diffraction (SAED) pattern of as-prepared AuCu alloy NCs. Experimental data are compared with the database powder XRD pattern for tetragonal AuCu (JCPDS No. 01-071-5024). (e–h) High-angle annular dark field-scanning TEM (HAADF-STEM) image and corresponding quantitative EDX maps (intensity proportional to atomic percent) for Au and Cu, showing homogeneous distribution of the two elements for NCs in the starting colloidal sample. The noise observed outside the NCs is caused by irradiation-induced carbon contamination, caused by the presence of residual organics.

areas including hundreds of NCs of the same sample agree with the XRD results (Figure 1d). On the basis of the results of structural characterization, it can be additionally concluded that NC sintering must have occurred during the AuCu synthesis, likely during the annealing step at 280 °C, which is essential to obtain an ordered AuCu alloy, as demonstrated by Chen et al.[10] In the absence of NC sintering, the starting Au NCs with an average size of 3.1 nm would indeed evolve to ~3.7 nm AuCu NCs and not to 6.1 nm, as measured for the synthesized AuCu NCs (see the Supporting Information for additional details on calculations). Further evidence of alloy formation was provided by comparison of the visible light absorption spectra of the Au and AuCu NCs, shown in Figure S3 in the Supporting Information. Consistent with alloy formation, the plasmon peak of Au at 520 nm was shifted toward the plasmon peak of Cu at 561 nm by about 27 nm in the case of the AuCu (atomic Au:Cu = 50:50) alloy NCs, in line with what has been reported in the literature.[10,13]

2.2. Catalytic Activity Results. To evaluate the catalytic activity of the synthesized AuCu NCs in the CO oxidation, the NCs were deposited on γ-Al_2O_3 and exposed to different activation treatments prior to catalytic tests, following the procedures described in detail in the Experimental Section. The transient activity of 1 wt % AuCu/Al_2O_3 catalyst in CO oxidation for three runs, each of them performed after the oxidizing pretreatment, is shown in Figure 2a. On investigation

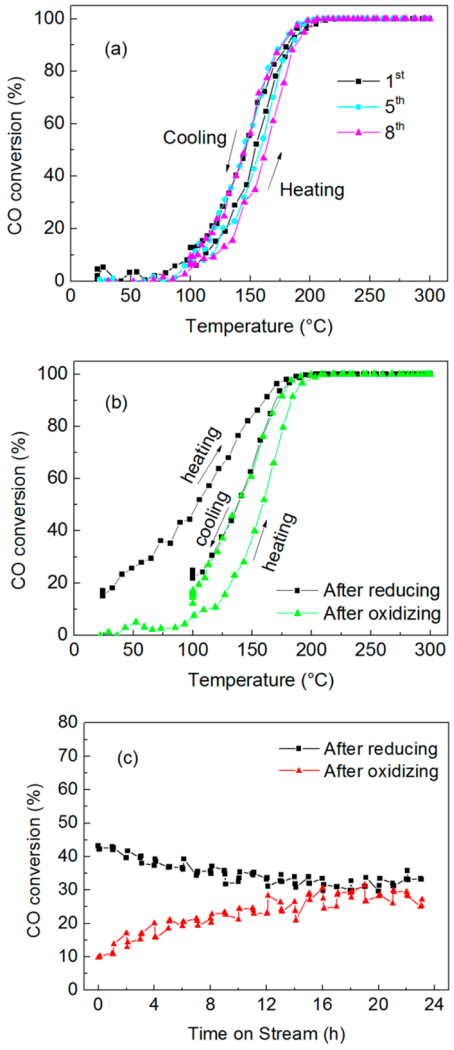

Figure 2. Catalytic activity data for the 1 wt % AuCu/Al_2O_3 catalyst in CO oxidation: (a) catalytic activity during three reaction cycles (first, fifth, and eighth) after the oxidizing pretreatment; (b) catalytic activity after oxidizing and reducing pretreatments; (c) steady-state activity data at a constant temperature of 100 °C after oxidizing and reducing pretreatments. Conditions: CO 1% v/v; O_2 6% v/v; GHSV = 3000000 Ncc/(h (g of AuCu)).

of the black square dots (first test after the initial activation procedure described in the Experimental Section), it can be noted that, during the heating phase of the experiments, the catalyst was almost inactive at low temperature and then the conversion gradually increased with temperature and reached 100% at a temperature of ~200 °C. During the cooling phase of the test, the catalytic activity decreased with temperature, resulting in a small but evident hysteresis, so that the activity at a given temperature during the cooling phase was higher than that in the heating phase. Figure 2a reports the first, fifth, and eighth reaction cycles performed after the oxidizing pretreatment on the same catalyst batch. A comparison among the three curves provides useful information about the stability of the catalyst with time on stream and about the effectiveness of the oxidizing pretreatments to restore the same surface

DOI: 10.1021/cs501923x
ACS Catal. 2015, 5, 2154–2163

situation after the catalytic tests. Indeed, the catalyst was initially activated under an oxidizing atmosphere after being loaded in the reactor, and then various series of tests were performed, exposing the catalyst to different pretreatments, i.e. oxidizing and reducing without any specific order, always followed by a reaction cycle. Regardless of the history of the sample, the activity toward CO oxidation after oxidizing pretreatment was extremely stable and reproducible, as supported by the data displayed in Figure 2a. Moreover, we observed a clear indication of synergy between Au and Cu by comparing the alumina-supported AuCu catalyst against a monometallic Au/Al_2O_3 catalyst (see Figure S4 in the Supporting Information). Even though we employed smaller Au NCs, which should be more active in CO oxidation, the synergy between Au and Cu led to a superior performance for the 6 nm AuCu NCs catalyst, especially at temperatures above 100 °C.

When the catalyst was pretreated according to the reducing protocol described in the Experimental Section, the catalytic activity in CO oxidation dramatically changed (Figure 2b). The sample exhibited about 15% conversion already at room temperature, corresponding to a significantly higher activity in comparison with that observed after the oxidizing pretreatment. The CO conversion then increased with temperature, approaching 100% at about 200 °C. During the following cooling phase of the test, the reduced sample exhibited a lower activity in comparison to the heating transient, resulting in a reverse hysteresis in comparison to the same sample after the oxidizing pretreatment. Interestingly, the catalytic activities during the cooling transients of both reduced and oxidized catalysts converged. When the sample was then heated again in a second reaction cycle without any further pretreatment, the catalytic activity in CO oxidation almost overlapped with that of the prior cooling transient (see Figure S5 in the Supporting Information), thus resulting in a performance closer to that observed after an oxidizing pretreatment.

In addition to the transient tests, the catalyst was also tested in CO oxidation at a constant temperature of 100 °C for 24 h (Figure 2c). The catalyst lost ~25% of its initial activity when the test followed the reducing pretreatment, approaching a conversion value of ~30% after 24 h of time on stream. The oxidized catalyst instead gained activity during 24 h of exposure to CO/O_2 atmosphere, eventually approaching the same conversion value as the reduced catalyst after 24 h.

To benchmark the catalytic activity of the prepared sample, we evaluated the initial CO oxidation rate at 25 °C after reducing pretreatment. As shown in Table 1, the synthesized catalyst sample, when pretreated according to the reducing protocol, exhibited a CO oxidation rate which was comparable to those reported for $AuCu/TiO_2$[3d] and $AuCu/SiO_2$[3a] catalysts under similar conditions.

Table 1. Comparison of CO Oxidation Rates for AuCu Catalysts

catalyst	temp (°C)	CO oxidation rate (mol of CO/(g_{Au}/h))	source
$AuCu/Al_2O_3$	25	0.30	this work
$AuCu/TiO_2$	20	0.27	ref 3d
$AuCu/SiO_2$	25	0.43	ref 3a

2.3. Characterization of the $AuCu/Al_2O_3$ Catalyst. In order to shed light on the catalytic activity changes observed upon the applied pretreatments, as well as upon exposure to reaction atmosphere, we characterized the $AuCu/Al_2O_3$ catalyst by means of TEM and CO/NO adsorption in situ diffuse reflectance infrared Fourier transform spectroscopy (DRIFTS) at three different stages: namely, after oxidation pretreatment, after reducing pretreatment, and after a reaction cycle. Overview STEM-HAADF images of the catalyst in the three mentioned conditions are reported in Figure S6 in the Supporting Information. For the three conditions, we observed a homogeneous distribution of the NCs on the surface of the alumina grains, with no evident differences in the NC sizes for the different treatments. Despite the presence of few larger particles, highlighted by the asymmetric size distribution reported in Figure S6d–f, we can conclude that the initial size distribution of the NCs was essentially preserved. Additionally, the extremely stable catalytic activity measured during the entire catalyst testing period indirectly proved the absence of significant sintering phenomena with time on stream, in line with what has already been reported in the literature on the effect of Cu in increasing the stability and sintering resistance of AuCu catalysts.[3a−d,4a]

Furthermore, the transformations of the AuCu NCs were followed locally after oxidizing or reducing pretreatments and after one cycle of reaction by STEM-EDX (see Figure 3a–c). After oxidizing activation, Au was localized within the NCs while a diffuse signal from Cu was observed over all of the alumina support. This result is in contrast with the speculation of Sandoval et al.[3d] about the migration of Cu atoms and the

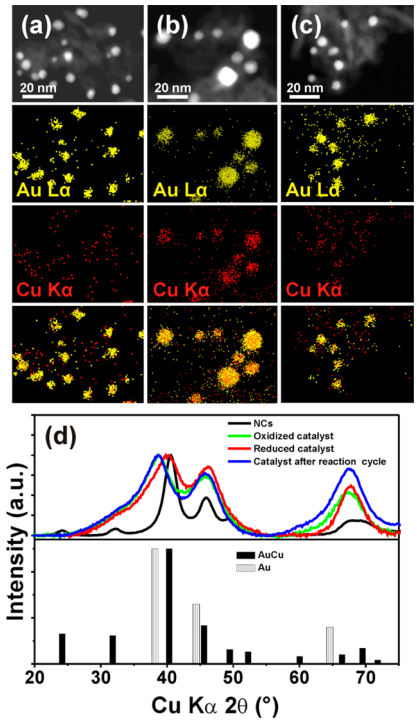

Figure 3. HAADF-STEM images and corresponding quantitative EDX maps (intensity proportional to atomic percent) for Au and Cu after (a) oxidizing pretreatment, (b) reducing pretreatment, and (c) reaction cycle. (d) Azimuthally integrated, background-subtracted SAED patterns of the 1 wt % $AuCu/Al_2O_3$ catalyst after oxidation, after reduction, and after one cycle of reaction, in comparison to AuCu colloidal NCs. The experimental patterns are compared to database powder XRD patterns for Au (JCPDS No. 00-004-0784) and AuCu (JCPDS No. 01-071-5024).

DOI: 10.1021/cs501923x
ACS Catal. 2015, 5, 2154−2163

following formation and accumulation of Cu oxide under the Au particles after such oxidizing treatment. In contrast, both Au and Cu are localized within the particles after the reducing pretreatment, with a weak Cu signal detected on the support. After one cycle of reaction, an intermediate condition was observed, with Au clearly localized within the NCs and a slightly higher concentration of Cu within the NCs with respect to the support.

XRD analyses of the catalyst at the three different stages did not lead to conclusive results on the accompanying structural transformations involving the NCs, due to the proximity of the high-intensity peaks from γ-Al_2O_3 to the significant features from the metallic NCs and to the low volume fraction of the latter species (see Figure S7 in the Supporting Information). Because of its local character, SAED could instead follow the structural transformations for alumina grains characterized by a relatively high NC loading, albeit with a resolution and precision lower than those of XRD. SAED analyses of the catalyst in the three different stages, in comparison with the pattern obtained on the parent colloidal NCs, are reported in Figure 3d. After oxidizing activation, the diffraction peak positions matched those of Au, while after the following reducing pretreatment a cell contraction was observed. The comparison with the pattern obtained from the parent colloidal particles showed that the initial order of the AuCu tetragonal phase was lost at this stage, while the reduction treatment led to bimetallic NCs in a less ordered solid solution phase (face-centered cubic (fcc) structure), with about 46 atomic % Cu. Within the precision of SAED, no significant differences were observed in the patterns between the catalyst after the oxidizing treatment and after one cycle of reaction, suggesting that in the latter case the Cu atoms were not incorporated in the fcc structure of the Au NCs.

While TEM characterization provided useful information on the evolution of NC composition and structure upon the different treatments, DRIFTS tests were performed to track the evolution of metal oxidation states on the same samples. To do this, we selected two probe molecules, CO and NO, and studied their interaction with the catalyst surface. CO has indeed been reported to form carbonyl species on $Au^{\delta+}$, Au^0, Cu^0, and Cu^+,[14] while NO forms stable nitrosyl species selectively on Cu^{2+}.[14a] Figure 4a,b shows respectively the IR spectra in the carbonyl region after 10 s and 42 min of exposure to the carbon monoxide mixture at room temperature (for the same sample pretreated under either an oxidizing or a reducing atmosphere), while Figure 4c reports the IR spectra in the same region after 40 min of purging at room temperature under a He atmosphere. As can be seen, after 10 s of exposure (Figure 4a), the reduced sample exhibited a main peak at 2130 cm^{-1} with a shoulder at 2102 cm^{-1}, while the oxidized sample had only one peak at the bigger wavenumber of 2137 cm^{-1}. Considering that Cu^{2+} does not form carbonyl species at room temperature, the only band observed at 2137 cm^{-1} over the oxidized sample can be reasonably assigned to $Au^{\delta+}$–CO species.[15] This assignment was confirmed by performing CO adsorption on the monometallic Au/Al_2O_3 catalyst (see Figure S9a in the Supporting Information): a band was observed at 2142 cm^{-1} on the oxidized Au catalyst, in line with what was observed over the oxidized $AuCu/Al_2O_3$ catalyst. For the latter sample, the presence of Cu^+ carbonyl species was ruled out by monitoring the desorption phase of the experiment: Cu^+ is indeed reported to form carbonyl species that are stable at room temperature upon evacuation in the 2122–2132 cm^{-1} region.[3d,14a,b] After 40 min of purging in He, no residual carbonyl band could be observed, as shown in Figure 4c, indicating the absence of any Cu^+ species.

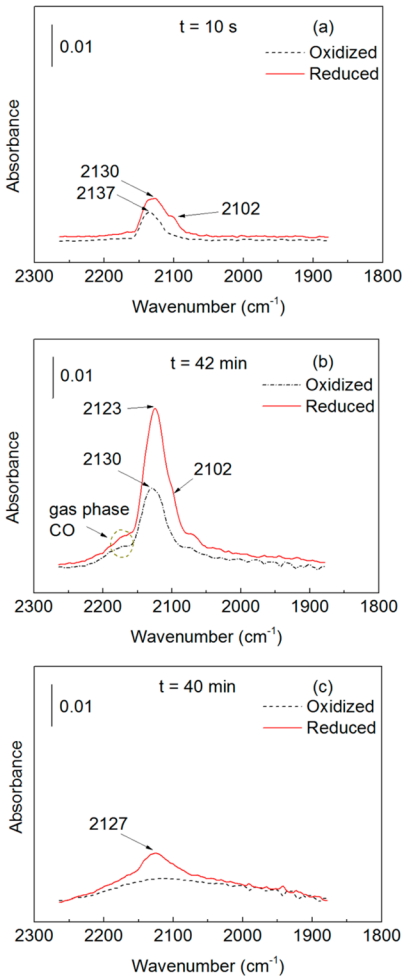

Figure 4. DRIFTS spectra in the carbonyl region recorded during the adsorption (a, b) and desorption (c) of CO at room temperature on the 1 wt % $AuCu/Al_2O_3$ catalyst. The sample was either oxidized (black dashed curves) or reduced (red curves) prior to the test. Spectra were taken after (a) 10 s and (b) 42 min of exposure to the probe gas (0.2% v/v CO, balance He) and after (c) 40 min of purging under a He atmosphere.

When the monometallic Au/Al_2O_3 catalyst underwent the reducing pretreatment, the following CO adsorption test resulted in the shift of the carbonyl band to 2116 cm^{-1} (see Figure S9b in the Supporting Information), in line with the shift reported in the literature from $Au^{\delta+}$ to Au^0.[3d,15] The shoulder at 2102 cm^{-1} on the reduced $AuCu/Al_2O_3$ catalyst can thus be attributed to Au^0, while the bands at 2130 and 2123 cm^{-1} in the case of the reduced catalyst can be assigned to Cu^+ or Cu^0, as they are both known to form carbonyl species at room temperature between 2122 and 2132 cm^{-1}.[14a,c,16] The dominant presence of Cu^0 is supported by SAED, which proves AuCu alloy formation. However, the presence of residual Cu^+ species was confirmed by monitoring the desorption phase of the experiment: as reported in Figure 4c, the reduced sample showed a residual carbonyl band even after 40 min of purging at room temperature, consistent with the formation of stable Cu^+ carbonyls.[14a] The reduced sample also exhibited higher intensities for the carbonyl bands, which can be a qualitative

DOI: 10.1021/cs501923x
ACS Catal. 2015, 5, 2154–2163

indication of higher capacity of the reduced sample for CO adsorption.

A comparison between the initial absorption after 10 s of exposure (Figure 4a) with the final absorption after 42 min (Figure 4b) indicates that, regardless of the type of pretreatment, the main peaks were slightly shifted to lower wavenumber by ~8−10 cm^{-1}, while the intensities of carbonyl species increased. Both trends are consistent with the increase of CO surface coverage with exposure time. The accumulation of CO in the gas phase is also evident by observing the evolution of the absorption at ~2170 cm^{-1}.

NO adsorption at room temperature was studied to detect the presence of Cu^{2+} on the surface of the catalyst after different pretreatments. The formation of nitrosyl species was monitored following the evolution of IR spectra in the 1800−2250 cm^{-1} range during 42 min of exposure to 650 ppm of NO in He. After 10 s of exposure, the absorption spectrum of the reduced catalyst (Figure 5a) was still almost flat, indicating no

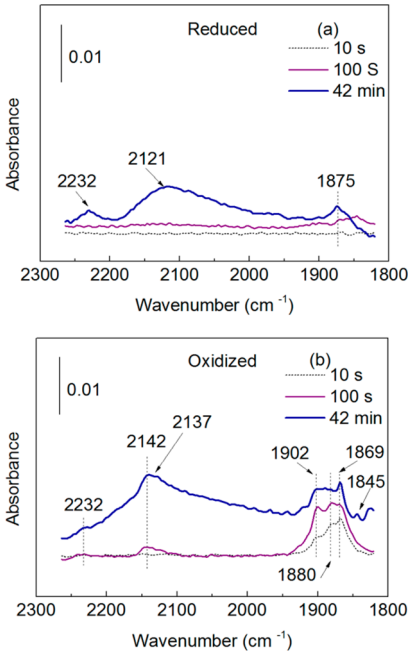

Figure 5. DRIFTS spectra in the nitrosyl region obtained during the adsorption of NO at room temperature on the 1 wt % $AuCu/Al_2O_3$ catalyst. Spectra were taken after 10 s, 100 s, and 42 min of exposure to the probe gas on the same sample that was either reduced (a) or oxidized (b) prior to the test. Probe gas composition: 650 ppm of NO, balance He.

adsorbed NO species and thus no Cu^{2+} on the catalyst surface. This is line with the reduction of Cu species inferred from the TPR test (see Figure S8 in the Supporting Information). However, after prolonged exposure to the NO stream, three main bands centered at around 1875, 2121, and 2232 cm^{-1} appeared. The first band can be assigned to Cu^{2+} nitrosyl species[14a] and the second and the third bands to the formation of respectively NO^+ and N_2O adsorbed on the alumina surface.[14a,17] The formation of these species is consistent with the presence of NO_2 contamination in the NO stream. Such a contamination likely arises from the disproportionation reaction of NO (3 NO ↔ N_2O + NO_2), which leads to the formation of N_2O and NO_2 (with the latter known to be a strong oxidizing agent) and which justifies the formation of Cu^{2+} nitrosyl species.[14a,18] NO DRIFTS on monometallic Au/Al_2O_3 catalyst (see Figure S10 in the Supporting Information) evidenced the same broad band at 2121 cm^{-1} for both oxidized and reduced catalysts, in line with the presence of NO_2 contamination, while no nitrosyl formation was detected on the same sample.

A different scenario was observed when the oxidized catalyst was exposed to NO. Figure 5b indeed shows several peaks in the region of 1910−1840 cm^{-1} already after 10 s of exposure to NO, indicating the formation of different Cu^{2+} nitrosyl species.[14a,18b] With longer exposure time, the intensity of the nitrosyl bands increased, accompanied by the formation of new features at around 2140 and 2232 cm^{-1}. In line with the assignments on the prereduced sample, these bands are assigned respectively to NO^+ and N_2O species.[14a,18b] The absence of nitrosyl species on Au was verified by means of a control experiment as specified above.

IR spectra were also taken after a CO oxidation reaction cycle, which was performed following an oxidizing or reducing pretreatment. Spectra of CO adsorption at room temperature after 100 s of exposure to the probe stream are shown in Figure 6. The oxidized and reduced catalysts after a CO oxidation

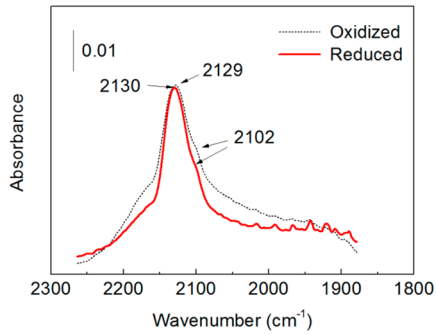

Figure 6. DRIFTS spectra in the carbonyl region obtained during the adsorption of CO at room temperature on the 1 wt % $AuCu/Al_2O_3$ catalyst. The sample was first either oxidized (black dashed curves) or reduced (red curves) and then exposed to a CO/O_2 reaction cycle prior to the adsorption test. Spectra were taken after 100 s of exposure to the probe gas (0.2% v/v CO, balance He).

reaction cycle have very similar spectral features: in both cases we observe one peak at ~2130 cm^{-1}, already attributed to $Au^{\delta+}/Cu^+/Cu^0$ carbonyls, as well as a shoulder at 2102 cm^{-1}, which is attributed to CO adsorption on Au^0. The various infrared band assignments are summarized in Scheme 2.

These results are in line with the catalytic activity tests. We have indeed shown that the CO oxidation catalytic activity of the catalyst after one cycle of reaction converged to the same value during the cooling phase of the transient reaction test,

Scheme 2. Infrared Band Assignments for Carbonyl and Nitrosyl Species Identified on the Catalyst Surface by Means of in Situ Diffuse Reflectance Infrared Fourier Transform Spectroscopy (DRIFTS)

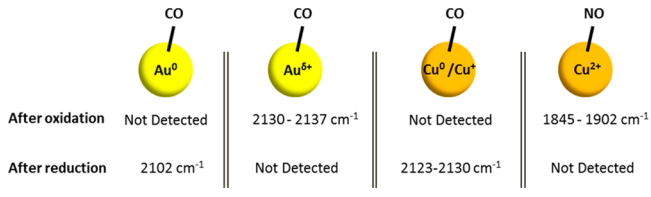

DOI: 10.1021/cs501923x
ACS Catal. 2015, 5, 2154−2163

Scheme 3. Sketch of the AuCu NC Transformations as a Function of the Activation Treatment and Reaction Environment: (Top) Starting AuCu NCs after Colloidal Deposition; (Bottom Left) after Oxidizing Pretreatment; (Bottom Center) after Reaction Cycle; (Bottom Right) after Reducing Pretreatment

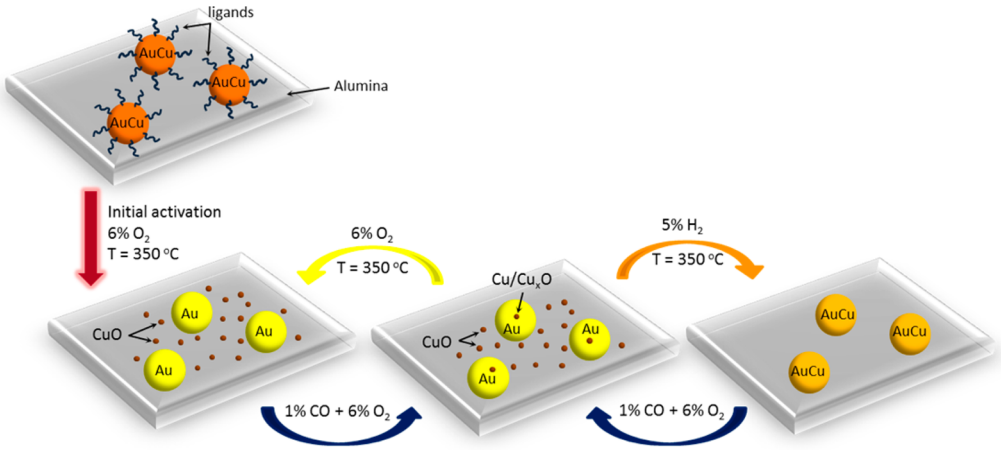

regardless of oxidizing or reducing pretreatments (Figure 2). Consistently, DRIFTS tests indicated that the same surface species were detected after a reaction cycle, independently from the initial condition of the catalyst.

3. DISCUSSION

The supported bimetallic AuCu NCs underwent structural changes upon exposure to different gas atmospheres. On the basis of our TEM and DRIFTS studies, we can deduce that exposing the catalytic system to reducing or oxidizing environments led to two opposite scenarios: while a reducing treatment led to the formation of AuCu disordered alloy NCs (Scheme 3, bottom right image), a strongly oxidizing treatment caused a phase segregation between gold and copper. While gold remained localized in NC entities, copper was finely dispersed on the support (in this case Al_2O_3), likely in the form of oxide clusters (Scheme 3, bottom left image). The presence of Cu^{2+} (e.g., CuO) was supported by combined CO and NO adsorption DRIFTS studies. We observed the formation of different Cu^{2+}−nitrosyl species, indicating the existence of different Cu^{2+} sites on the surface. Considering the high dispersion of Cu on the support surface, different nitrosyl species can result from oxide clusters localized in different chemical environments (e.g., CuO localized on or close to Au NCs, isolated CuO clusters on Al_2O_3).

The different situations observed on the catalyst surface after oxidizing or reducing pretreatments resulted in a dramatic change of the catalyst performance, indicating a strong structure/activity relationship for the studied catalytic system. The phase segregation between Au and Cu and the migration of the latter on the alumina support observed after the oxidizing pretreatment was found to be detrimental to the catalytic activity in CO oxidation. This is in line with many literature reports on Au-catalyzed CO oxidation, where the presence of an interface between gold and a reducible metal oxide is considered as the catalytically active region of the catalyst surface.[7,19] In agreement with this interpretation, the intimate contact between Au and Cu in the alloyed NCs obtained with a reducing treatment (Scheme 3, bottom right image) boosted the CO conversion.[3a,d] Our data support the hypothesis that exposure to the reactive atmosphere (mostly oxidizing due to the presence of a large excess of O_2) resulted in the sudden formation of CuO clusters/patches in intimate contact with the Au surface: the adsorption and activation of oxygen provided by Cu then enhanced the catalytic activity.[2a,3a,b,4b] Increasing the temperature under the same atmosphere then resulted in the progressive migration of Cu on the support and the subsequent decrease of catalytic activity (Scheme 3, bottom center image). In contrast, when starting from a fully oxidized situation (Scheme 3, bottom left image), exposure to the reactive atmosphere (partially reducing due to the presence of CO) resulted in the partial back-migration of Cu to the Au NCs (Scheme 3, bottom center image), leading then to a slightly enhanced activity during the cooling transient of the test. In agreement with this interpretation, the performance of the same sample in a second reaction cycle, carried out without the application of any pretreatment, almost overlaps with that observed during the cooling transient of the first cycle (Figure S5 in the Supporting Information). Interestingly, these structural changes were significant at temperatures as low as 100 °C, even though their kinetics were slow: indeed after 18−20 h at 100 °C under the same reaction atmosphere, the same catalytic activity was approached, regardless of the initial situation of the catalyst surface. Consistently, the same situation was observed on the catalyst surface, as probed by CO adsorption monitored by DRIFTS.

The reproducibility of the catalytic activity data during noninterrupted cycles of pretreatment/test proved both the stability of the synthesized material and the effectiveness of the applied pretreatments in restoring the same surface situation, independently from the catalyst pretreatment/test history.

The observed process of phase segregation caused by exposure to different atmospheres has often been reported in the case of bimetallic catalysts.[20] This segregation was shown to be size and support dependent;[20c] thus, different results can be expected by changing the size of the NCs and the support where the NCs are deposited. The observed process of copper migration on the alumina surface, evidently driven by temperature and gas composition, can also be strongly influenced by the support material, thus leading to different situations even when applying the same pretreatment protocols. These aspects need to be further explored in future works, in order to rationalize the effect of different pretreatments on the catalytic activity of AuCu catalysts.

DOI: 10.1021/cs501923x
ACS Catal. 2015, 5, 2154−2163

4. CONCLUSIONS

We studied the transformations that colloidal AuCu ordered phase NCs supported on Al_2O_3 underwent upon different redox treatments and correlated such changes with the catalytic activity in the CO oxidation reaction. By means of different characterization techniques we highlighted a phase segregation between gold and copper upon a high-temperature (350 °C) oxidizing treatment. Copper was found to be finely dispersed on the support, likely in the form of oxide clusters, while gold remained localized in the NCs. The weak interaction between the two metals resulted in poor CO oxidation activity. However, a high-temperature (350 °C) reducing treatment was able to restore the AuCu alloyed NCs, albeit in the form of a solid solution, face-centered cubic phase. The intimate contact between the two metals was most likely the reason for a significant enhancement of the CO oxidation catalytic activity. We also observed that the CO/O_2 reacting atmosphere affected the composition of the NCs: as a result, also the CO oxidation reaction rate changed with time on stream, even at temperatures as low as 100 °C. These transformations were fully reversible, with alloyed AuCu NCs restored upon the high-temperature reducing treatment, regardless of the catalyst history.

5. EXPERIMENTAL SECTION

5.1. NC Synthesis and Catalyst Preparation. Au NCs (3 nm) were synthesized using the procedure reported in ref 8 with some modifications, specifically in the synthesis temperature and washing procedure. Typically, 100 mg of $HAuCl_4 \cdot 3H_2O$ (Sigma-Aldrich) was mixed with 10 mL of oleylamine (OlAm, Sigma-Aldrich 70%) and 10 mL of 1,2,3,4-tetrahydronaphthalene (Tetralin, Sigma-Aldrich) and degassed under an inert atmosphere of N_2 for 30 min. Then, 0.5 mmol of *tert*-butylamine–borane complex (TBAB, Sigma-Aldrich), 1 mL of OlAm, and 1 mL of Tetralin were mixed and sonicated until a clear solution was formed. The solution was injected into the Au precursor mixture at 21 °C, and stirring was maintained for 1 h. After the reaction, a solution of 2-propanol and ethanol (4/1 v/v) was added and the particles were precipitated by centrifugation. The supernatant was discarded and the precipitate dispersed in hexane. This washing procedure was repeated one more time before the NCs were dispersed in 10 mL of hexane. The colloidal solution was stable for at least 2 months, as observed by TEM analyses (not reported).

The as-prepared 3 nm Au NCs were used as seeds to synthesize AuCu NCs (target Au/Cu = 50/50 atomic ratio). Typically, 7 mg of $CuCl_2$ dihydrate (99+%, Alfa Aesar) was dissolved in a mixture of 3 mL of OlAm and 0.5 mL of oleic acid (OlAc, Sigma-Aldrich), and this mixture was magnetically stirred under a N_2 blanket at 100 °C until the copper salt was completely dissolved. Then 8 mg of Au NCs was added to the bluish solution of the Cu precursor and subjected to vacuum at 80 °C for 1 h to remove the hexane. Subsequently, the temperature of the mixture was increased to 280 °C with a heating rate of 5 °C/min under an N_2 atmosphere. After 1 h at this temperature, the solution was cooled to room temperature, diluted with 2 mL of anhydrous toluene, and transferred to a glovebox (Ar atmosphere). Here the NCs were washed twice by addition of a 2-propanol/methanol solution (1/3 v/v) and centrifugation. The final product was collected and dispersed in 2 mL of anhydrous hexane. The alumina-supported AuCu catalyst was prepared by colloidal deposition, which is known to preserve the particle size distribution of the parent colloidal NCs after deposition.[7] Typically, the AuCu colloidal solution (target AuCu NCs load 1 wt %) was added to γ-Al_2O_3 powder (extrudate from Sigma-Aldrich, crushed and sieved to 90 μm mean particles size, BET specific surface area 190 m^2/g), dispersed in hexane, and magnetically stirred for 2 h. Subsequently, the suspension was dried under an N_2 atmosphere and the resulting powder was calcined at 200 °C for 13 h.

5.2. Catalytic Experiments. The catalytic activity of the catalysts for CO oxidation was measured using a micro reactor system coupled with a micro-gas chromatograph (μ-GC) equipped with three thermal conductivity detectors (TCD) to analyze CO, O_2, and CO_2 (SRA Instruments Model R-3000). Typically, the catalyst powder was diluted with alumina (2/1 weight ratio) and loaded into a quartz reactor. The feed gas was a mixture of 1% v/v CO and 6% v/v O_2 balanced with He with a flow rate of 80 Ncc/min corresponding to a gas hourly space velocity of 3000000 Ncc/(h (g of Au + Cu)). After loading, the catalyst was initially activated at 350 °C for 10 h in 6% v/v O_2 in He to remove organic ligands present on the NC surface. Independent thermogravimetric analysis (TGA; see Figure S11 in the Supporting Information) showed that weight loss due to organic ligand removal was completed at 350 °C. For the activity measurements, the reactor was heated from room temperature to 300 °C with a heating rate of 2 °C/min, kept at 300 °C for 30 min, and then cooled to 100 °C with the same rate and kept at 100 °C for 30 min. Transient activity data were collected every 4 min during the mentioned cycle of the catalytic test. In addition to the first activation treatment to remove organic ligands, before each test the catalyst was exposed to either a reducing (5% v/v H_2 in He) or an oxidizing (6% v/v O_2 in He) atmosphere at a temperature of 350 °C for 1 h. The heating rate used in activation, reducing, and oxidizing pretreatments was set to 5 °C/min. Long-term steady-state catalytic activity data were also collected after reducing and after oxidizing pretreatments: in both cases, the pretreated catalyst was exposed to the reactants at a constant temperature of 100 °C for 24 h using the same feed gas composition and space velocity of the transient tests. Three measurements were performed on the outlet stream every 1 h to monitor the evolution of the catalytic activity with time on stream.

5.3. Characterization. *5.3.1. TEM.* Overview BF-TEM and SAED patterns were acquired on various samples using a JEOL JEM-1011 microscope with a thermionic W source operated at 100 kV. The SAED patterns were acquired at constant camera length after mechanically adjusting the height of the sample to the eucentric height and after carefully focusing the NC images. In the same session, the diffraction camera length and the system distortions were calibrated using a nanocrystalline Au sputtered film on a standard C-covered Cu grid. The elaboration of SAED patterns (beam-stop removal, centering, azimuthal integration, and background subtraction) was carried out using the PASAD software.[21]

HRTEM and HAADF-STEM analyses were performed using a JEOL JEM-2200FS microscope equipped with a Schottky emitter operated at 200 kV, a CEOS spherical aberration corrector of the objective lens, and an in-column Omega filter. Compositional analysis of the AuCu alloy NCs deposited on alumina was carried out by EDX performed in STEM mode with a Bruker Quantax 400 system with a 60 mm^2 silicon-drift detector (SDD). Quantification of the Au/Cu atomic ratio from the collected EDX spectra by the Cliff–Lorimer ratio

DOI: 10.1021/cs501923x
ACS Catal. 2015, 5, 2154–2163

method systematically led to overestimation of the Au content due to a spurious Au fluorescence signal originating within the detecting system. In any case the Cliff−Lorimer ratio method was applied to obtain semiquantitative intensity scaling in the two-dimensional elemental maps. For TEM analyses, ∼10 mg of the catalyst powder samples was suspended in 1 mL of anhydrous chloroform and mildly sonicated. About 100 μL of the supernatant was then deposited onto a carbon-coated metal grid. For EDX analyses, non-Cu grids (W for the oxidized catalyst, Mo for the remaining samples) and an analytical holder with a Be cup were used. For the as-synthesized NCs, about 100 μL of diluted AuCu colloidal solution was deposited onto the carbon support film.

5.3.2. HRSEM-EDX. Analyses were carried out using a JEOL JSM-7500FA instrument, equipped with an Oxford X-max LN_2-free SDD, with 80 mm^2 of sensor active area and 129 eV of energy resolution at 5.9 keV (Mn Kα). Samples were prepared by drop-casting the alloy NC solution on an ultrasmooth silicon wafer. The extended Pouchou and Pichoir (XPP) matrix correction algorithm included in the Oxford AZtec software was used to analyze the data.

5.3.3. Elemental Analysis. The chemical composition of the colloidal NCs as well as the metal loadings of the catalyst were measured by ICP-AES using a Varian Vista AX spectrometer. Samples were dissolved in HCl/HNO_3 3/1 (v/v) overnight, diluted with deionized water (14 μS), and filtered using a PTFE filter before measurement.

5.3.4. XRD. Measurements were performed using a Rigaku SmartLab X-ray diffractometer equipped with a 9 kW Cu Kα (l = 1.542 Å) rotating anode, operating at 40 kV and 150 mA. A Göbel mirror was used to convert the divergent X-ray beam into a parallel beam and to suppress the Cu Kβ radiation (λ = 1.392 Å). A zero diffraction silicon substrate was used to collect XRD spectra on both colloidal NCs solutions and catalyst powdered samples. The diffraction patterns were collected at room temperature over an angular range of 10−85°, with a step size of 0.05°. XRD data analysis was carried out using PDXL 2.1 software from Rigaku.

5.3.5. In Situ DRIFTS. Spectra were collected using a Vertex 70 infrared spectrometer (Brüker Optics) equipped with a DRIFTS cell (Praying Mantis, Harrick) and a MCT detector, cooled with liquid nitrogen. The outlet of the DRIFTS cell was connected to an online mass spectrometer (Omnistar, Pfeiffer). Using a four-port selector valve, it was possible to switch between two different gas streams, one used for purging and/or pretreatments and the other containing the probe species. The loaded sample was pretreated under oxidizing or reducing atmospheres prior to the test. The pretreatments followed the same conditions used in the case of catalytic experiments, except for the heating rate, which was set to 20 °C/min. After each pretreatment, the cell was cooled to room temperature. Once the temperature was stabilized, the background spectrum was collected while the pretreatment mixture was continuously flowed. Then, the flowing gas was switched to a mixture containing either 0.2% v/v CO or 650 ppm of NO with a balance of He. Spectra were collected every 10 s for the first 100 s of adsorption. The process was monitored for a further 40 min, collecting a spectrum every 10 min. After that, the flow was switched to a He stream to purge the catalyst and desorption spectra were collected during 40 min of purging with inert gas. Each test was repeated at least two times to verify the reproducibility of the measurement. The spectra of CO adsorption at room temperature was also collected after performing one cycle of reaction in the DRIFTS cell, using the same feed composition and flow rate as in the case of catalytic experiments. When NO was used as the probe molecule, a reducing treatment at high temperature (5% H_2, balance He at 350 °C) was always performed after the adsorption test to clean the surface from nitrite/nitrate species. Then, the desired pretreatment and the following adsorption test were performed.

■ ASSOCIATED CONTENT

Supporting Information

The following file is available free of charge on the ACS Publications website at DOI: 10.1021/cs501923x.

BF-TEM of as-prepared Au NCs, SEM EDX maps of AuCu NCs, calculation of AuCu NC size on the basis of starting Au NC size, optical absorption characterization of Au and AuCu NCs, comparison of activity for 3 nm Au/Al_2O_3 vs 6 nm $AuCu/Al_2O_3$, activity of the AuCu catalyst after one cycle of reaction without performing any pretreatment, overview HAADF-STEM images, XRD pattern and TPR measurement on the $AuCu/Al_2O_3$ catalyst sample, CO and NO DRIFTS on the Au/Al_2O_3 catalyst sample, and TGA data of the AuCu NCs in air (PDF)

■ AUTHOR INFORMATION

Corresponding Authors

*E-mail for L.M.: liberato.manna@iit.it.

*E-mail for M.C.: massimo.colombo@iit.it

Present Address

†(For P.G.) Catalonia Energy Research Institute − IREC, Jardí de les Dones de Negre 1, Sant Adria del Besos, Spain

Notes

The authors declare no competing financial interest.

■ ACKNOWLEDGMENTS

The authors acknowledge financial support from European Union through the EU-ITN network Mag(net)icFun (PITN-GA-2012−290248) and the Italian FIRB grant "Ossidi Nanostrutturati" (contract #RBAP115AYN).

■ REFERENCES

(1) (a) Tao, F. *Chem. Soc. Rev.* **2012**, *41*, 7977−7979. (b) Jiang, H.-L.; Xu, Q. *J. Mater. Chem.* **2011**, *21*, 13705−13725. (c) Sankar, M.; Dimitratos, N.; Miedziak, P. J.; Wells, P. P.; Kiely, C. J.; Hutchings, G. J. *Chem. Soc. Rev.* **2012**, *41*, 8099−8139.

(2) (a) Wang, A.; Liu, X. Y.; Mou, C.-Y.; Zhang, T. *J. Catal.* **2013**, *308*, 258−271. (b) Bracey, C. L.; Ellis, P. R.; Hutchings, G. J. *Chem. Soc. Rev.* **2009**, *38*, 2231−43.

(3) (a) Liu, X.; Wang, A.; Wang, X.; Mou, C. Y.; Zhang, T. *Chem. Commun.* **2008**, 3187−9. (b) Liu, X.; Wang, A.; Zhang, T.; Su, D.-S.; Mou, C.-Y. *Catal. Today* **2011**, *160*, 103−108. (c) Mozer, T. S.; Dziuba, D. A.; Vieira, C. T. P.; Passos, F. B. *J. Power Sources* **2009**, *187*, 209−215. (d) Sandoval, A.; Louis, C.; Zanella, R. *Appl. Catal., B* **2013**, *140−141*, 363−377. (e) Bauer, J. C.; Mullins, D. R.; Oyola, Y.; Overbury, S. H.; Dai, S. *Catal. Lett.* **2013**, *143*, 926−935. (f) Liu, J.-H.; Wang, A.-Q.; Chi, Y.-S.; Lin, H.-P.; Mou, C.-Y. *J. Phys. Chem. B* **2004**, *109*, 40−43.

(4) (a) Li, X.; Fang, S. S. S.; Teo, J.; Foo, Y. L.; Borgna, A.; Lin, M.; Zhong, Z. *ACS Catal.* **2012**, *2*, 360−369. (b) Liu, X.; Wang, A.; Li, L.; Zhang, T.; Mou, C.-Y.; Lee, J.-F. *J. Catal.* **2011**, *278*, 288−296. (c) Petkov, V.; Shastri, S.; Shan, S.; Joseph, P.; Luo, J.; Zhong, C.-J.; Nakamura, T.; Herbani, Y.; Sato, S. *J. Phys. Chem. C* **2013**, *117*, 22131−22141.

DOI: 10.1021/cs501923x
ACS Catal. 2015, 5, 2154−2163

(5) Bauer, J. C.; Mullins, D.; Li, M.; Wu, Z.; Payzant, E. A.; Overbury, S. H.; Dai, S. *Phys. Chem. Chem. Phys.* **2011**, *13*, 2571−81.
(6) Yin, J.; Shan, S.; Yang, L.; Mott, D.; Malis, O.; Petkov, V.; Cai, F.; Shan, N. M.; Luo, J.; Chen, B. H.; Engelhard, M.; Zhong, C.-J. *Chem. Mater.* **2012**, *24*, 4662−4674.
(7) Comotti, M.; Li, W.-C.; Spliethoff, B.; Schüth, F. *J. Am. Chem. Soc.* **2005**, *128*, 917−924.
(8) Peng, S.; Lee, Y.; Wang, C.; Yin, H.; Dai, S.; Sun, S. *Nano Res.* **2008**, *1*, 229−234.
(9) Jia, C.-J.; Schuth, F. *Phys. Chem. Chem. Phys.* **2011**, *13*, 2457−2487.
(10) Chen, W.; Yu, R.; Li, L.; Wang, A.; Peng, Q.; Li, Y. *Angew. Chem., Int. Ed. Engl.* **2010**, *49*, 2917−21.
(11) Mourdikoudis, S.; Liz-Marzán, L. M. *Chem. Mater.* **2013**, *25*, 1465−1476.
(12) Okamoto, H.; Chakrabarti, D. J.; Laughlin, D. E.; Massalski, T. B. *J. Phase Equilib.* **1987**, *8*, 454−474.
(13) (a) Motl, N. E.; Ewusi-Annan, E.; Sines, I. T.; Jensen, L.; Schaak, R. E. *J. Phys. Chem. C* **2010**, *114*, 19263−19269. (b) Sra, A. K.; Schaak, R. E. *J. Am. Chem. Soc.* **2004**, *126*, 6667−6672.
(14) (a) Hadjiivanov, K.; Knözinger, H. *Phys. Chem. Chem. Phys.* **2001**, *3*, 1132−1137. (b) Venkov, T.; Hadjiivanov, K. *Catal. Commun.* **2003**, *4*, 209−213. (c) Dulaurent, O.; Courtois, X.; Perrichon, V.; Bianchi, D. *J. Phys. Chem. B* **2000**, *104*, 6001−6011.
(15) Mihaylov, M.; Knözinger, H.; Hadjiivanov, K.; Gates, B. C. *Chem. Ing. Technol.* **2007**, *79*, 795−806.
(16) (a) Praliaud, H.; Mikhailenko, S.; Chajar, Z.; Primet, M. *Appl. Catal., B* **1998**, *16*, 359−374. (b) Dandekar, A.; Vannice, M. A. *J. Catal.* **1998**, *178*, 621−639.
(17) (a) Venkov, T.; Hadjiivanov, K.; Klissurski, D. *Phys. Chem. Chem. Phys.* **2002**, *4*, 2443−2448. (b) Morterra, C.; Boccuzzi, F.; Coluccia, S.; Ghiotti, G. *J. Catal.* **1980**, *65*, 231−234. (c) Parres-Esclapez, S.; Such-Basañez, I.; Illán-Gómez, M. J.; Salinas-Martínez de Lecea, C.; Bueno-López, A. *J. Catal.* **2010**, *276*, 390−401.
(18) (a) Shimokawabe, M.; Okumura, K.; Ono, H.; Takezawa, N. *React. Kinet. Catal. Lett.* **2001**, *73*, 267−274. (b) Hadjiivanov, K.; Saussey, J.; Freysz, J. L.; Lavalley, J. C. *Catal. Lett.* **1998**, *52*, 103−108.
(19) (a) Lopez, N. *J. Catal.* **2004**, *223*, 232−235. (b) Schubert, M. M.; Hackenberg, S.; van Veen, A. C.; Muhler, M.; Plzak, V.; Behm, R. J. *J. Catal.* **2001**, *197*, 113−122.
(20) (a) Ma, T.; Fu, Q.; Su, H.-Y.; Liu, H.-Y.; Cui, Y.; Wang, Z.; Mu, R.-T.; Li, W.-X.; Bao, X.-H. *ChemPhysChem* **2009**, *10*, 1013−1016. (b) Mayrhofer, K. J. J.; Juhart, V.; Hartl, K.; Hanzlik, M.; Arenz, M. *Angew. Chem., Int. Ed.* **2009**, *48*, 3529−3531. (c) Guisbiers, G.; Mejia-Rosales, S.; Khanal, S.; Ruiz-Zepeda, F.; Whetten, R. L.; José-Yacaman, M. *Nano Lett.* **2014**, *14*, 6718−6726.
(21) Gammer, C.; Mangler, C.; Rentenberger, C.; Karnthaler, H. P. *Scr. Mater.* **2010**, *63*, 312−315.

DOI: 10.1021/cs501923x
ACS Catal. 2015, 5, 2154−2163